atmosphere

MDPI

Article

Surface Gravity Wave Effect on Hurricane Energetics

Yalin Fan * and Zhitao Yu

Naval Research Laboratory, Stennis Space Center, Hancock County, MS 39529, USA; zhitao.yu@nrlssc.navy.mil
* Correspondence: yalin.fan@nrlssc.navy.mil

Abstract: Theoretical researches have established that the energy dynamics of a mature tropical cyclone may be idealized to be very similar to a theoretical Carnot heat engine. Assuming the dissipative heating of the atmospheric boundary layer and the net production of mechanical energy in the cyclone dominate the energy budget of the storm, the potential maximum wind speed of the cyclone can be approximated as a function of the air–sea temperature difference ($T_s - T_0$) and specific enthalpy $(k_0^* - k)$ difference: $|V_{max}|^2 \approx \frac{C_k}{C_D}\frac{T_s - T_0}{T_0}(k_0^* - k)$. Although this theory gives a straighforward estimate of maximum tropical cyclone intensity, studies found that few real storms achieve this theoretical maximum estimated using climatological atmospheric conditions and sea surface temperatures. The discrepancies were attributed to a lack of knowledge of the values of the drag coefficient (C_D) and surface exchange coefficient for enthalpy (C_k), and on insufficient upper ocean thermal measurements under hurricanes. Recent observational and numerical studies have unearthed another possible factor for these discrepancies by showing that the energy flux into surface gravity waves under extreme wind conditions can be an order of magnitude greater than formerly believed, and thus may play an important role in the energy budget of tropical cyclones. In this study, numerical experiments are performed to investigate the effect of surface gravity waves under a range of idealized tropical cyclone winds. The wave fields are simulated using the WAVEWATCH III model. Our results demonstrate that by considering the energy flux to surface gravity waves, the potential maximum wind speed can be reduced by up to 12% and this ratio varies with the storm size, intensity, and translation speed.

Keywords: surface gravity wave; tropical cyclone; intensity

Citation: Fan, Y.; Yu, Z. Surface Gravity Wave Effect on Hurricane Energetics. *Atmosphere* **2022**, *13*, 279. https://doi.org/10.3390/atmos13020279

Academic Editor: Xiangbo Feng

Received: 10 January 2022
Accepted: 2 February 2022
Published: 7 February 2022

1. Introduction

Tropical cyclones, also popularly known as hurricanes or typhoons, are among the most spectacular and deadly geophysical phenomena. Both of the most lethal and the most expensive natural disasters in U.S. history were tropical cyclones [1]. The basic source of energy for tropical cyclones is heat transfer from the ocean, as first recognized by Riehl [2] and Kleischmidt [3]. The mature tropical cyclone may be idealized as a steady, axisymmetric flow whose energy cycle is very similar to that of an ideal Carnot engine [4]. Thus, like the Carnot cycle, the energy cycle of a mature tropical cyclone is one of isothermal expansion, adiabatic expansion, isothermal compression, and adiabatic compression. Hence, the upper limit of the intensity of a tropical cyclone is dictated by the balance between energy generation by surface fluxes and dissipation, and can be estimated using the temperature difference ($T_s - T_0$) and specific enthalpy difference ($k_0^* - k$) between the ocean surface and troposphere [5]. Although this theory gives a straighforward estimate of tropical cyclone intensity, studies found that few real storms achieve this theoretical maximum estimated using climatological atmospheric conditions and sea surface temperatures [6]. The author attributes the discrepancies to the lack of knowledge of the values of the drag coefficient and surface exchange coefficient for enthalpy, and on insufficient upper ocean thermal measurements under hurricanes.

Direct measurements of the fluxes that produce the surface exchange coefficient, such as the drag coefficient, have been made at wind speeds as large as 25 m/s, but

technical problems have so far prevented reliable estimates at higher speeds [1]. As a result, momentum transfer under extreme wind conditions has been extrapolated from these field measurements in a variety of modeling applications, including hurricane risk assessment and prediction of storm motion, intensity, waves, and storm surges. However, studies found that the intensity of simulated hurricanes is very sensitive to the details of the spray formulation, as well as to the surface gravity wave induced drag [7].

The energy flux into the surface gravity waves was formerly perceived to be negligible; however, observations and numerical studies have revealed that the energy flux into ocean surface gravity waves is an order of magnitude greater than formerly believed [8,9], especially under hurricane conditions [10,11]. In the study, we investigate the importance of the surface gravity waves on hurricane intensity using the Carnot engine theory through estimations of the percentage of energy flux into surface gravity waves relative to the net production of mechanical energy under a range of tropical cyclone categories and sizes.

The outline of this paper is as follows: modifications to the energy cycle of a mature tropical cyclone based on the ideal Carnot engine theory to include the effect of surface gravity waves are formulated in Section 2, model description and a brief outline of the experimental design are introduced in Section 3, the results are presented in Section 4, and a summary of this study and discussions are presented in Section 5.

2. The Surface Wave Factor in the Energy Cycle of a Mature Tropical Cyclone

In the ideal Carnot engine theory, both the heat input and the dissipation of kinetic energy (KE) in this cycle occur largely through air–sea transfer [4]. By including the dissipative heating in the thermodynamic energy cyclone of the storm, Bister and Emanuel [5] were able to provide a more accurate estimation of maximum wind speed for tropical cyclones. In their theory, the flux of enthalpy from the sea is quantified using bulk formulae of the form:

$$F_k = C_k \rho_{air} |V| (k_0^* - k) \tag{1}$$

and the vertically integrated dissipative heating of the atmospheric boundary layer can be modeled as:

$$D_{air} = C_D \rho_{air} |V|^3 \tag{2}$$

where V is the near-surface wind speed, ρ_{air} is the air density, k is the specific enthalpy of air near the surface, k_0^* is the enthalpy of the air in contact with the ocean, assumed to be saturated with water vapor at ocean temperature, and C_D and C_k are the transfer coefficients of momentum and enthalpy.

Assuming the kinetic energy used to generate ocean currents and surface gravity waves is negligible, the work (mechanical energy) generated by transferring thermal energy from the hot source can be modeled as:

$$P = 2\pi \frac{T_s - T_0}{T_s} \int_a^b [F_k + D_{air}] r dr \tag{3}$$

where T_s is the sea surface temperature, T_0 is the temperature at the tropopause, and the integral is taken over the first leg of the cyclone.

The net energy dissipation is:

$$D_{net} = 2\pi \int_a^b D_{air} r dr \tag{4}$$

Letting $P = D_{net}$ lead to:

$$2\pi \frac{T_s - T_0}{T_s} \int_a^b [F_k + D] r dr = 2\pi \int_a^b C_D \rho_{air} |V|^3 r dr \tag{5}$$

If we assume that the integrals in Equation (5) are dominated by the values of their integrands near the radius of maximum wind, the potential maximum wind speed can be expressed as:

$$|V_{max}|^2 \approx \frac{C_k}{C_D}\frac{T_s - T_0}{T_0}(k_0^* - k) \tag{6}$$

Although the kinetic energy used to generate ocean currents remains negligible, recent studies based on the integration of the full surface gravity wave spectrum, however, have shown that the energy flux into ocean surface gravity waves (D_{wave}) is an order of magnitude greater than what people formerly believed [8–10]. If we assume the energy that is taken out of the atmosphere to generate ocean surface gravity waves is a portion R of the dissipative heating of the atmospheric boundary layer D_{air}, so that $D_{wave} = RD_{air}$, then total work generated and net energy dissipation become:

$$P^w = 2\pi\frac{T_s - T_0}{T_s}\int_a^b [F_k + (1+R)D_{air}]rdr \tag{7}$$

and

$$D_{net}^w = 2\pi\int_a^b (1+R)D_{air}rdr \tag{8}$$

where the superscript w indicates the term has included the effect of surface gravity wave.

Letting P^w equals to D_{net}^w, and follow the procedures to obtain Equation (6), we get:

$$|V_{max}^w|^2 \approx \frac{C_k}{C_D}\frac{T_s - T_0}{(1+R)T_0}(k_0^* - k) \tag{9}$$

This is the new estimate of potential maximum wind speed with the effect of surface gravity waves. Its ratio to the traditional estimation without considering the surface wave effect is:

$$\frac{|V_{max}^w|^2}{|V_{max}|^2} = \frac{1}{1+R} \tag{10}$$

Since we know that the wind stress τ can be estimated as $\tau = C_D\rho_{air}|V|^2 = \rho_{air}u_*^2$ (in which u_* is the friction velocity), substitute this into Equation (2) for D_{air}, and assume that both D_{air} and D_{wave} are dominated by the values of their integrands near the radius of maximum wind (RMW), the ratio of D_{wave} and D_{air} can be expressed as:

$$R = \frac{D_{wave}}{D_{air}}\bigg|_{RMW} = \frac{D_{wave}}{\rho_{air}u_*^2|V_{max}|} \tag{11}$$

where D_{wave} can be calculated through the integration of the source function in all frequencies and directions following Fan and Hwang [11]. Equation (11) will be used to estimate R in the experiments described in Section 3.

3. Wave Model and Experimental Design

3.1. The Wave Model

The wind-wave model, WAVEWATCH III® (WWIII) version 4.18, developed and used operationally at the National Centers for Environmental Prediction (NCEP) [12] is used for this study. WWIII computes the evolution in space and time of the wave spectrum, which for the present study is discretized using 45 directions and 38 intrinsic (relative) frequencies extending from 0.02855 to 0.97 Hz, with a logarithmic increment of f(n + 1) = 1.1f(n), where f(n) is the nth frequency. The wave model is built on a latitude-longitude grid with a horizontal resolution of 1/12° degree.

Ocean wave modeling is a very useful and convenient way to obtain the spatial and temporal distribution of directional wave spectra without the limitations associated with measurements, although the model output may differ from observations because of uncertainties in wind input, model physics, and numeric. During the past 4 decades,

considerable improvements have been made in predicting ocean wave directional spectra. Third-generation wave models such as WWIII have been used to study surface wave responses during tropical cyclones and the modeled wave parameters (significant wave height, mean/dominant wave length, mean/dominant wave direction) are shown to compare well with observations [13–18].

In this study, the energy flux into surface gravity waves D_{wave} is calculated through the integration of the model input source function in all frequencies and directions and u_* is produced by the ST4 source package in WWIII. Thus, we can estimate R from Equation (11) for all experiments detailed in Section 3.2 below.

3.2. Experimental Design

Idealized stationary and moving tropical cyclone (TC) experiments are conducted to study the variation of the surface gravity wave effect on the potential maximum wind speed caused by the changes in the TC parameters (Table 1): stationary TC experiments set A varies the radius of maximum wind speed (RMW) from 50 km to 90 km with a fixed maximum wind speed (MWS) of 45 ms^{-1}; in stationary TC experiments set B the MWS varies from 35 ms^{-1} to 55 ms^{-1} with a fixed RMW of 30, 70, and 90 km respectively; the effect of different TC translation speed (TSP) is investigated in experiments set C by moving the axisymmetric TC with a constant TSP of 5 ms^{-1} and 10 ms^{-1}. The Holland analytical model [19] is used to prescribe the axisymmetric wind field (Figure 1) in the TC experiments with given input parameters of the MWS and RMW in Table 1 and the central and ambient pressure set to 1012 hPa and 968 hPa, respectively, for all experiments.

Table 1. Experimental designs of the TC experiments. Here, TSP, MWS, and RMW denote translation speed, maximum wind speed, and radius of maximum winds of the TC, respectively.

Experiment	TSP (ms^{-1})	MWS (ms^{-1})	RMW (km)
A	0	45	30, 40, 50, 60, 70, 80, 90
B	0	35, 40, 45, 50, 55	30
	0	35, 40, 45, 50, 55	70
	0	35, 40, 45, 50, 55	90
C	5, 10	45	70

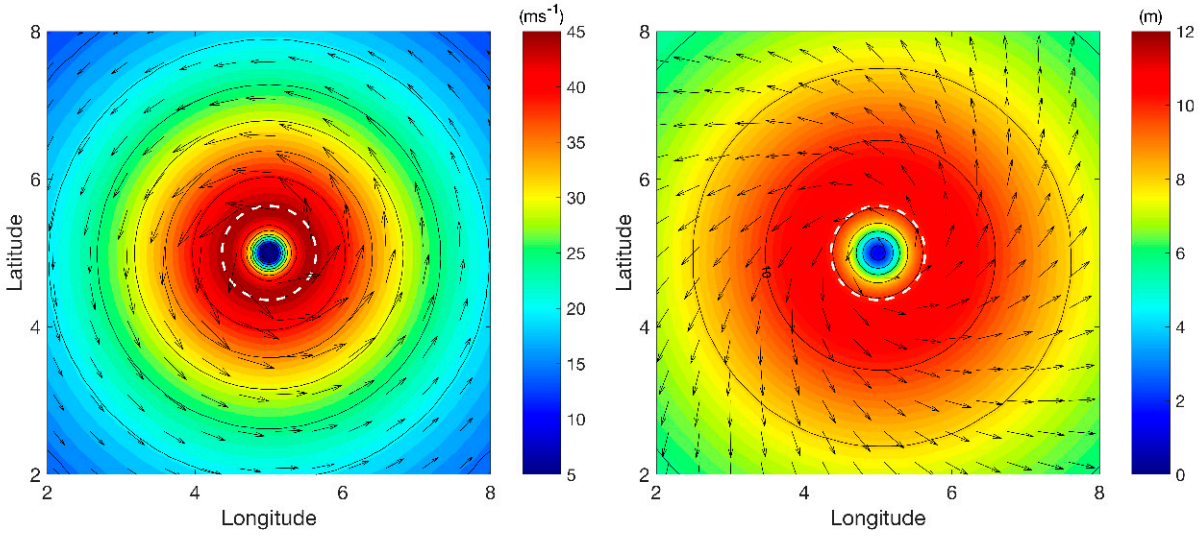

Figure 1. (**left**) Wind field in experiment A with RMW = 70 km. The arrows indicate wind speed vector, the color scales indicate wind speed magnitude (ms $^{-1}$), and the contours are given at every 5 ms $^{-1}$. (**right**) Wave field under the stationary TC: the arrows indicate dominant wave direction, the color scales indicate significant wave height (m), and the contours are given at every 2 m. The dashed white line in both figures give the location of RMW.

The WWIII model domain is set to be 10° in latitude and 10° in longitude for the stationary TC experiments, and 18° in longitude and 30° in latitude for the moving TC experiments. In all experiments, the grid increment is 1/12° in both directions and the time increment is 100 s. The water depth is set to 4000 m for the whole domain so that the surface gravity waves have no interaction with the seafloor. All results are presented after a spin-up time of 54 h, when a quasi-steady state is achieved [10]. In the case of a moving TC a quasi-steady state is achieved relative to the TC center.

4. Results

Because both the wind field and the wave field are axisymmetric (Figure 1) in all stationary TC experiments [10], the results in experiments set A and B are analyzed along one of the radii.

4.1. Variation of $\frac{V_{max}^{w}}{V_{max}}$ with Radius of Maximum Wind

The variation of the ratio V_{max}^{w} to V_{max} with different radii of maximum wind is explored in experiment A. As shown in Figure 2a, the effect of surface gravity waves on the reduction of the potential maximum wind speed linearly increases with the radius of maximum wind speed. This is because, under a TC wind field, the effective fetch (the distance over which the spectral components in the vicinity of the spectral peak have been exposed to the wind as they propagate) increases as the RMW increases [10]. Hence, the total energy in the waves field (often represented by the significant wave height) and, therefore, the total energy flux into the wave field D_{wave} also increase with the increase of RMW. Since u_* barely changes with RMW given the same maximum wind speed V_{max}, R increases with RMW according to Equation (11). Thus, the ratio of V_{max}^{w} to V_{max} decreases with the increase of R according to Equation (10) and follows a linear regression of:

$$\frac{V_{max}^{w}}{V_{max}} = -2 \times 10^{-4} RMW + 0.9167 \quad (12)$$

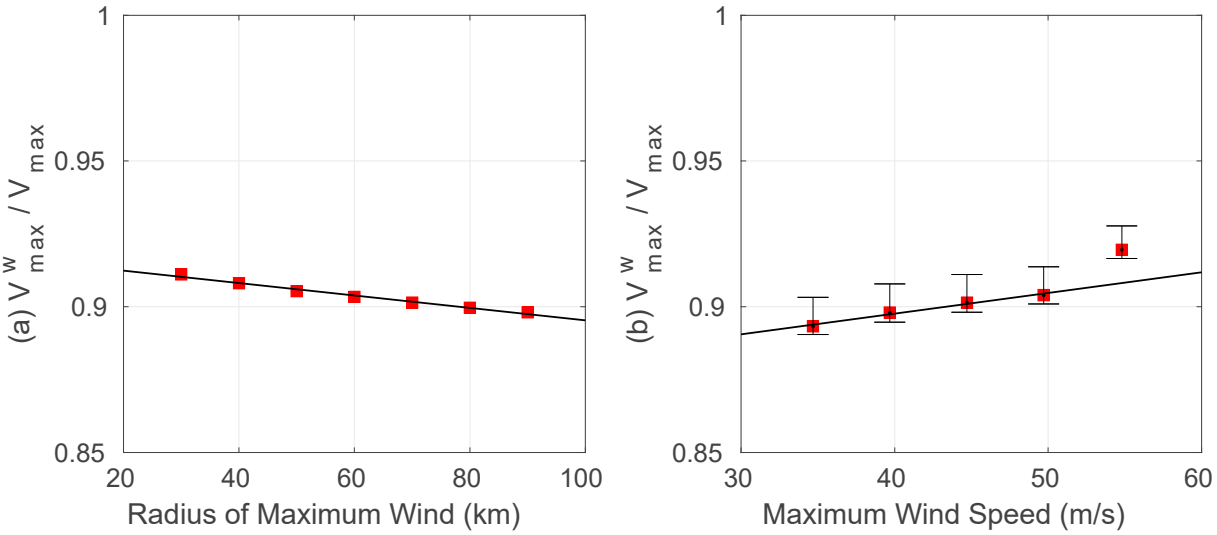

Figure 2. The ratio of V_{max}^{w} to V_{max} (**a**) at different radius of maximum wind (red square) in experiment A, and (**b**) at different maximum wind speed and radius of maximum wind speed in experiment B with the red squares representing the ratios for TCs with a radius of maximum wind of 70 km. The upper and lower limits of the error bar in (**b**) indicate the ratio values for TCs with a radius of maximum wind of 90 and 30 km, respectively. In both figures, the black lines give the linear regression of the ratios.

4.2. Variation of $\frac{V_{max}^{w}}{V_{max}}$ with Maximum Wind Speed

The variation of the ratio V_{max}^{w} to V_{max} with different maximum wind speeds is explored in experiment B. Unlike in experiment A, this ratio increases with MWS indicating the effect of surface gravity waves reduces as the storm becomes stronger (Figure 2b). For MWS up to 50 m/s, a linear relationship is found between $\frac{V_{max}^{w}}{V_{max}}$ and the MWS:

$$\frac{V_{max}^{w}}{V_{max}} = 7 \times 10^{-4}\text{MWS} + 0.8693 \quad (13)$$

This is consistent with Fan and Hwang [11] who investigated the kinetic energy flux budget under TCs with intensity up to category 3 on the Saffir-Simpson scale. They found that as the MWS increases, the rate of increase in the total energy flux into the wave field D_{wave} and u_*^2 are comparable with each other, thus the variation of R depends purely on the variation of V_{max} according to Equation (11) and decreases with the increase of MWS, and hence lead to the increase of ratio V_{max}^{w} to V_{max} with the increase of MWS according to Equation (10).

However, the result at MWS = 55 m/s appears to be an outlier. Its different behavior was caused by the capping of roughness length z_0 in the wave model based on extensive global and regional evaluations of model results. A maximum value of 1.002 is set for z_0 in WWIII because it provides the best results at global scale when using ECMWF winds [12]. While u_*^2 steadily increases with the MWS at low to medium storm intensity, its magnitude ceases to increase shortly after the MWS exceeds 50 m/s (Figure 3b) due to the capping of z_0. Since the wave energy spectrum computed by the wave models is from a balance between input and dissipation, the choice of friction velocity cap will influence the well-tuned wave growth behavior in the model [11], and the estimated energy flux budget will apparently respond to the change of behavior in u_*^2. Furthermore, in the Holland TC wind model, the wind profile significantly varies with the MWS if the pressure difference and RMW is kept constant: as the MWS increases, the wind speed increases/decreases more rapidly inside/outside of the RMW (Figure 3a). The strong wind forcing becomes more localized near the RMW and thus reduces the effective fetch for wave growth. As a result of the capped u_*^2 and reduced fetch, D_{wave} decreased around the eyewall for the TC with MWS = 55 m/s and became even lower than the value for TC with a MWS of 50 m/s (Figure 3c). The combined effect of EF_w reduction and capping of u_*^2 has resulted in a strong decrease in R and, thus, a sudden increase in $\frac{V_{max}^{w}}{V_{max}}$.

The error bars in Figure 2b shows the range of $\frac{V_{max}^{w}}{V_{max}}$ between RMW of 30 km and 90 km. It suggests the effects of surface gravity waves on the storm potential intensity have the same behavior for different storm sizes with a reduction/increase of the ratio for smaller/larger storm sizes.

4.3. Moving Storm

The variation of the ratio $\frac{V_{max}^{w}}{V_{max}}$ under axisymmetric moving TCs is investigated in Experiment C with the storm moving northward at a constant speed of 5 and 10 m/s.

Due to the resonance effect caused by the movement of the TC, the surface waves are higher and longer in the front-right quadrant of the storm track and lower and shorter in the rear-left quadrant. Since the wave field becomes asymmetric under moving TCs, we expect the effect of surface gravity waves on TC potential intensity to be different at different locations around the eyewall. Thus, the model results are analyzed around the eyewall at every 5 degrees anticlockwise from the east (i.e., 90° is to the north of the storm center) in Figure 4. The potential intensity of the storm is reduced the most in the front quadrant with the ratio $\frac{V_{max}^{w}}{V_{max}}$ becoming as low as 0.875 in the faster moving storm. In the left quadrant of the storm, however, this ratio is higher than that in the stationary TC (dashed black line in Figure 4), and the faster the storm moves, the higher the ratio is. This is because when the translation speed of the storm increases, the wave height and length differences between the front-right and rear-left quadrants increase too. When the translation speed of

the storm approaches or exceeds the group velocity of the dominant waves (between 8 and 10 m/s), the waves in the front-right quadrant of the TC become "trapped" within the TC and thus produce the ultimate resonance effect. Although the analysis is presented here at every 5 degrees around the eyewall, most TCs in the real word have their maximum wind located in the right front quadrant of the storm, thus, we would expect a reduction in potential intensity (potential maximum wind speed) of 10 to 12% because of the effect of surface gravity waves on moving storms.

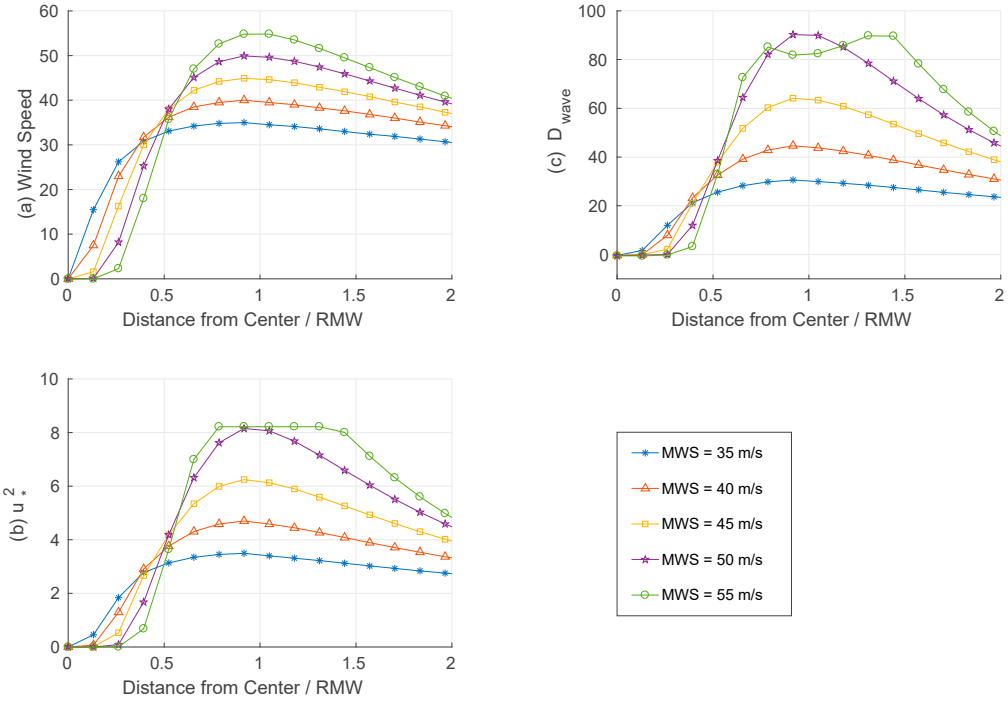

Figure 3. (**a**) Wind profile, (**b**) friction velocity squared u_*^2, and (**c**) total energy flux into the wave field D_{wave} vs. normalized distance from the center in Experiment B with RMW = 70 km.

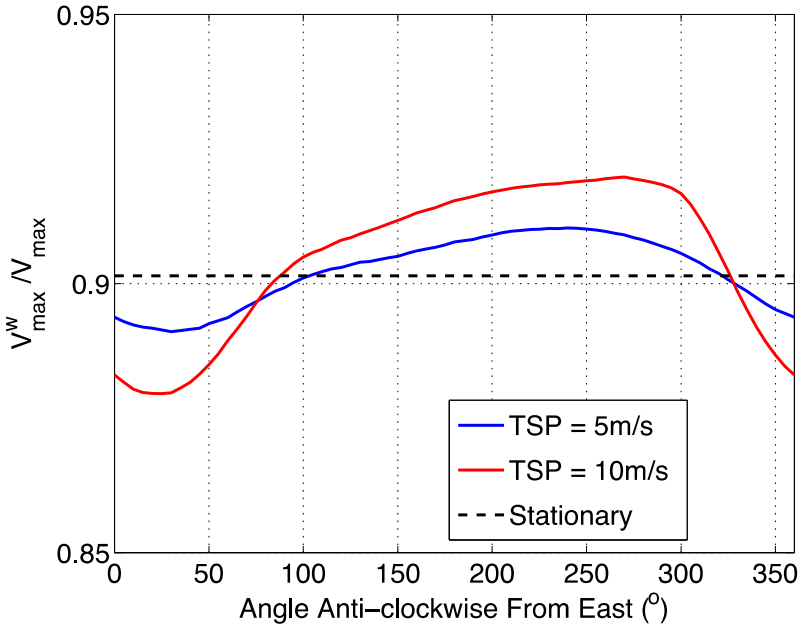

Figure 4. The ratio of V_{max}^{w} to V_{max} at every 5 degrees around the eyewall anti-clockwise from the east. The blue and red lines represent results from experiment C with TC translation speed of 5 and 10 m/s. The dashed black line gives results from experiment A with RMW = 70 km.

5. Summary and Discussions

In this study, numerical experiments are performed to investigate the effect of surface gravity waves on the reduction of potential intensity under a range of idealized tropical cyclone winds. The wave fields are simulated using the WAVEWATCH III (WWIII) model. Our results have demonstrated that by considering the energy flux to surface gravity waves, the theoretical potential maximum wind speed can be reduced by up to 12%, and this ratio varies with the storm size, intensity, and translation speed.

There are many limitations to this study. First, since the wave energy spectrum computed by the wave models is from a balance between input and dissipation, the estimated total energy flux into the wave field D_{wave} and the friction velocity u_* both depend on the source and dissipation functions chosen for the model simulations. There are several source functions implemented in WWIII. The most used ones for wave simulations under tropical cyclone (TC) forcing are ST3 [20–22], ST4 [23], and ST6 [24–26]. Liu et al. [27] evaluated the performance of these source function packages through intensive comparisons with satellite altimeter measurements, scanning radar altimeter measurements, and buoy observations during hurricane Ivan in 2004. The ST4 (used for the analysis in this study) and ST6 packages show similar skills in wave simulations and have both implement mechanisms to reduce drag coefficient, and thus u_* at high winds following field and laboratory observations [28–32]. ST4 is adapted from Janssen [21] and Bidlot et al. [20,33] with a reduction of u_* (hence, drag coefficient C_D) implemented by reducing the wind input for high frequencies and high winds and allowing a balance with a saturation-based dissipation. ST6 is developed based on Donelan et al. [34] with constraints on the wind input from air-flow separation, wave steepness, and wave breaking. Fan and Hwang [11] found that while the energy budget shows the same behavior between model results using the two source packages, the friction velocity calculated by the ST6 package is much lower than that calculated by the ST4 package at high winds. Thus, we would expect a larger R (Equation (11)) and hence a stronger reduction in potential maximum wind speed if ST6 is used for the analysis.

Second, the current study is limited to deep water only so that the waves will have no interaction with the bottom, which greatly simplified our budget calculation, but our findings may not apply to shallow and intermediate water depths when bottom friction become an important player in dissipation.

Finally, all calculations are performed using the stand-alone WWIII model. To clarify the physical processes, the condition is simplified such that the wind is not allowed to vary based on the sea state and no ocean currents are considered. However, evolving wind and current fields in realistic weather may result in significant differences in the energy fluxes between the atmosphere and the surface gravity wave field and, hence, affect the estimation on the relative importance of surface waves on the potential intensity estimation.

Author Contributions: Formal analysis, Y.F.; Investigation, Z.Y.; Writing–original draft, Y.F.; Writing–review & editing, Z.Y. All authors have read and agreed to the published version of the manuscript.

Funding: This research was funded by the Office of Naval Research under program element 062435N.

Institutional Review Board Statement: This paper is a contribution of NRL/JA/7320-22-5435, and has been approved for public release.

Informed Consent Statement: Not applicable.

Data Availability Statement: Not applicable.

Conflicts of Interest: The authors declare no conflict of interest.

References

1. Emanuel, K. Tropical Cyclones. *Annu. Rev. Earth Planet. Sci.* **2003**, *31*, 75–104. [CrossRef]
2. Riehl, H. A Model of Hurricane Formation. *J. Appl. Phys.* **1950**, *21*, 917–925. [CrossRef]
3. Kleinschmidt, E., Jr. Gundlagen einer theorie des tropischen zyklonen. *Arch. Meteorol. Geophys. Bioklimatol. Ser. A* **1951**, *4*, 53–72. [CrossRef]

4. Emanuel, K.A. An air-sea interaction theory for tropical cyclones. Part I. *J. Atmos. Sci.* **1986**, *42*, 1062–1071. [CrossRef]
5. Bister, M.; Emanuel, K.A. Dissipative heating and hurricane intensity. *Meteorol. Atmos. Phys.* **1998**, *50*, 233–240. [CrossRef]
6. Emanuel, K. A Statistical Analysis of Tropical Cyclone Intensity. *Mon. Weather Rev.* **2000**, *128*, 1139–1152. [CrossRef]
7. Andreas, E.L.; Emanuel, K.A. Effects of sea spray on tropical cyclone intensity. *J. Atmos. Sci.* **2001**, *58*, 3741–3751. [CrossRef]
8. Drennan, W.M.; Donelan, M.A.; Terray, E.A.; Katsaros, K.B. Oceanic Turbulence Dissipation Measurements in SWADE. *J. Phys. Oceanogr.* **1996**, *26*, 808–815. [CrossRef]
9. Terray, E.; Donelan, M.; Agrawal, Y.; Drennan, W.; Kahma, K.; Williams, A.; Hwang, P.; Kitaigorodskii, S. Estimates of Kinetic Energy Dissipation under Breaking Waves. *J. Phys. Oceanogr.* **1996**, *26*, 792–807. [CrossRef]
10. Fan, Y.; Ginis, I.; Hara, T. Momentum Flux Budget across the Air–Sea Interface under Uniform and Tropical Cyclone Winds. *J. Phys. Oceanogr.* **2010**, *40*, 2221–2242. [CrossRef]
11. Fan, Y.; Hwang, P. Kinetic energy flux budget across air-sea interface. *Ocean Model.* **2017**, *120*, 27–40. [CrossRef]
12. Tolman, H.L. WAVEWATCHIII Development Group, 2014: User Manual and System Documentation of WAVEWATCH III version® 4.18. Available online: https://polar.ncep.noaa.gov/waves/wavewatch/manual.v4.18.pdf (accessed on 1 February 2022).
13. Allard, R.; Rogers, E.; Martin, P.; Jensen, T.; Chu, P.; Campbell, T.; Dykes, J.; Smith, T.; Choi, J.; Gravois, U. The US navy coupled ocean-wave prediction system. *Oceanography* **2014**, *27*, 92–103. [CrossRef]
14. Fan, Y.; Ginis, I.; Hara, T.; Wright, C.W.; Walsh, E.J. Numerical Simulations and Observations of Surface Wave Fields under an Extreme Tropical Cyclone. *J. Phys. Oceanogr.* **2009**, *39*, 2097–2116. [CrossRef]
15. Fan, Y.; Rogers, W. Drag coefficient comparisons between observed and model simulated directional wave spectra under hurricane conditions. *Ocean Model.* **2016**, *102*, 1–13. [CrossRef]
16. Moon, I.-J.; Ginis, I.; Hara, T.; Tolman, H.L.; Wright, C.W.; Walsh, E.J. Numerical Simulation of Sea Surface Directional Wave Spectra under Hurricane Wind Forcing. *J. Phys. Oceanogr.* **2003**, *33*, 1680–1706. [CrossRef]
17. Phadke, A.C.; Martino, C.D.; Cheung, K.F.; Houston, S.H. Modeling of tropical cyclone winds and waves for emergency management. *Ocean Eng.* **2003**, *30*, 553–578. [CrossRef]
18. Xu, F.; Perrie, W.; Toulany, B.; Smith, P.C. Wind-generated waves in Hurricane Juan. *Ocean Model.* **2007**, *16*, 188–205. [CrossRef]
19. Holland, G.J. An analytic model of the wind and pressure profiles in hurricanes. *Mon. Wea. Rev.* **1980**, *108*, 1212–1218. [CrossRef]
20. Bidlot, J.-R.; Janssen, P.; Abdalla, S. *A Revised Formulation of Ocean Wave Dissipation and Its Model Impact*; ECMWF: Reading, UK, 2007; p. 27.
21. Janssen, P.A.E.M. Quasi-linear theory of wind wave generation applied to wave forecasting. *J. Phys. Oceanogr.* **1991**, *21*, 1631–1642. [CrossRef]
22. Janssen, P. *The Interaction of Ocean Waves and Wind*; Cambridge University Press: Cambridge, UK, 2004.
23. Ardhuin, F.; Rogers, W.E.; Babanin, A.V.; Filipot, J.; Magne, R.; Roland, A.; van der Westhuysen, A.; Queffeulou, P.; Lefevre, J.; Aouf, L.; et al. Semiempirical dissipation source functions for ocean waves. Part I: Definition, calibration, and validation. *J. Phys. Oceanogr.* **2010**, *40*, 1917–1941. [CrossRef]
24. Babanin, A.V. *Breaking and Dissipation of Ocean Surface Waves*; Cambridge University Press: Cambridge, UK, 2011.
25. Rogers, W.E.; Babanin, A.V.; Wang, D.W. Observation-Consistent Input and Whitecapping Dissipation in a Model for Wind-Generated Surface Waves: Description and Simple Calculations. *J. Atmos. Ocean. Tech.* **2012**, *29*, 1329–1346. [CrossRef]
26. Zieger, S.; Babanin, A.V.; Erick Rogers, W.; Young, I.R. Observation-based source terms in the third-generation wave model WAVEWATCH. *Ocean Model.* **2015**, *96*, 2–25. [CrossRef]
27. Liu, Q.; Babanin, A.; Fan, Y.; Zieger, S.; Guan, C.; Moon, I.-J. Numerical simulations of ocean surface waves under hurricane conditions: Assessment of existing model performance. *Ocean Model.* **2017**, *118*, 73–93. [CrossRef]
28. Donelan, M.A.; Haus, B.K.; Reul, N.; Plant, W.J.; Stiassnie, M.; Graber, H.C.; Brown, O.; Saltzman, E.S. On the limiting aerodynamic roughness of the ocean in very strong winds. *Geophys. Res. Lett.* **2004**, *31*, L18306. [CrossRef]
29. Powell, M.D.; Vickery, P.J.; Reinhold, T.A. Reduced drag coefficient for high wind speeds in tropical cyclones. *Nature* **2003**, *422*, 279–283. [CrossRef]
30. Takagaki, N.; Komori, S.; Suzuki, N.; Iwano, K.; Kuramoto, T.; Shimada, S.; Kurose, R.; Takahashi, K. Strong correlation between the drag coefficient and the shape of the wind sea spectrum over a broad range of wind speeds. *Geophys. Res. Lett.* **2012**, *39*, L23604. [CrossRef]
31. Takagaki, N.; Komori, S.; Suzuki, N. Estimation of friction velocity from the windwave spectrum at extremely high wind speeds. In *IOP Conference Series: Earth and Environmental Science*; IOP Publishing: Bristol, UK, 2016; Volume 35, p. 012009. [CrossRef]
32. Takagaki, N.; Komori, S.; Suzuki, N.; Iwano, K.; Kurose, R. Mechanism of drag coefficient saturation at strong wind speeds. *Geophys. Res. Lett.* **2016**, *43*, 9829–9835. [CrossRef]
33. Bidlot, J.-R.; Abdalla, S.; Janssen, P. *A Revised Formulation for Ocean Wave Dissipation in CY25R1*; ECMWF: Reading, UK, 2005; p. 35.
34. Donelan, M.A.; Babanin, A.V.; Young, I.R.; Banner, M.L. Wave-follower field measurements of the wind-input spectral function. Part II: Parameterization of the wind input. *J. Phys. Oceanogr.* **2006**, *36*, 1672–1689. [CrossRef]